ELSEVIER

Effect of large-scale periodic unsteadiness on the heat transport in the downstream region of a junction boundary layer

Donald Wroblewski
Department of Aerospace and Mechanical Engineering, Boston University, Boston, MA, USA

The heat transport in the boundary layer downstream of a junction between a streamlined cylinder and a wall is examined. This flow is characterized by large-scale periodic motions, attributable to vortex shedding, which affect the turbulent heat transport and may contribute to enhanced wall heat transfer. Experimental data obtained using a triple-wire turbulent heat-flux probe were analyzed using triple decomposition and a conditional sampling technique that separated the large-scale periodic motions from the background turbulence. The periodic motions lead to large-scale movements of the instantaneous thermal boundary-layer interface and contribute significantly to the overall Reynolds heat fluxes. The intermittency of the temperature signal revealed that the hot/cold interface penetrated much closer to the wall than in an undisturbed two-dimensional (2-D) boundary layer. Two different mechanisms that might be responsible for the observed transport phenomena are discussed: (1) a portion of the shed vortex filament that is skewed by the mean strain field of the wake and boundary layer; and (2) large counter-rotating streamwise vortices identified from mean-flow measurements that oscillate in the unsteady wake of the obstacle.

Keywords: junction boundary layers; unsteady flows; turbulent heat transport; conditional sampling

Introduction

Junction boundary layers arise, in some form or another, in various heat transfer applications, such as gas turbine blade end-wall heat transfer, cooling of protruding electronic chips, and plate fin heat exchangers. These flows are characterized by the interactions between a boundary layer developing along a surface and a wake developing in a perpendicular plane downstream of an obstacle attached to the wall (Figure 1). The three-dimensional (3-D) boundary layer downstream of the obstacle may be further complicated by the presence of horseshoe vortices and, for bluff obstacles such as cylinders, periodic shedding of Kármán vortices from the obstacle.

Much of the past work on junction flows has concentrated on characterizing the horseshoe vortex system that is formed when the approaching boundary layer encounters the leading edge of the obstacle. Baker (1980) and Goldstein and Karni (1984) have investigated the leading-edge region and characterized the formation of the horseshoe vortex system. Smith et al. (1992) showed that the vortices may be inherently unsteady. Extensive mean velocity and turbulence measurements have been made by Shabaka and Bradshaw (1981), McMahon et al. (1983), Mehta (1984), Merati et al. (1988), and Pierce and Harsh (1988), among others.

The region far downstream of the junction has received less attention. Rood and Keller (1984) observed large-scale organized motions, with a frequency well below the vortex-shedding frequency, in the boundary layer 10 chord lengths downstream of a streamlined wing–body junction.

The heat transfer in the region downstream of the obstacle wall junction has been the focus of several recent studies. Fisher and Eibeck (1990) measured Stanton numbers up to 10 diameters downstream of a circular cylinder and a tapered, but not fully streamlined, cylinder. These revealed increases over flat-plate Stanton numbers of up to 50%, the increase being attributed to the presence of the horseshoe vortex. Eibeck (1991) performed detailed mean velocity measurements in the same configurations investigated by Fisher and Eibeck. In these measurements, the secondary velocity field usually associated with the horseshoe vortex was absent behind the circular cylinder and at certain streamwise locations behind the tapered cylinder, but a larger vortex, with a rotation opposite to that of the expected horseshoe vortex, was a dominant feature of the secondary flow field. The absence of the horseshoe vortex suggested that another mechanism, possibly enhanced turbulent transport, could be responsible for the increased wall heat transfer.

Address reprint requests to Mr. D. Wroblewski, Department of Aerospace and Mechanical Engineering, Boston University, Boston, MA, USA.

Received 12 April 1994; accepted 6 September 1994

Int. J. Heat and Fluid Flow 17: 3–11, 1996

655 Avenue of the Americas, New York, NY 10010

0142-727X/96/$15.00
SSDI 0142-727X(95)00100-X

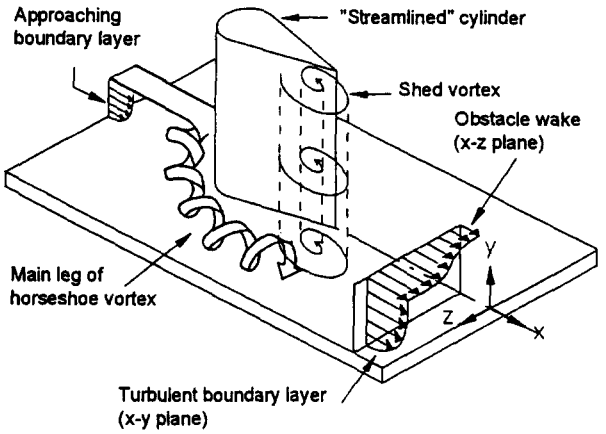

Figure 1 Schematic of junction boundary-layer flow.

Measurements of secondary velocities 14 and 28 diameters downstream of streamlined cylinders revealed that the counter-rotating vortices dominate the secondary flow field for an obstacle that spans the height of the wind tunnel, but are absent if the cylinder spans only half the height of the tunnel, in which case, a strong horseshoe vortex is present (Eibeck and Barland 1993). They suggest that the counter-rotating streamwise vortices arise from the tornado-like vortices that are normally vertically oriented and confined to the trailing edge of a finite-sized obstacle near a junction. For a full-height obstacle, the tornado-like vortices from the top and bottom junction interact and are swept downstream as streamwise vortices. An alternate mechanism for the development of these vortices is presented by Pauley (1993), who suggested that they are similar to passage vortices in gas-turbine blade cascades. He also indicates that they are a dominant factor in the wall heat transfer enhancement downstream of small-aspect ratio (height-to-diameter) obstacles.

Wroblewski and Eibeck (1992) experimentally studied the heat transport within the boundary layer 14 diameters downstream of a junction with a streamlined cylinder. Wall heat transfer enhancements, similar to those reported by Fisher and Eibeck (1990), were observed, along with corresponding increases in turbulent heat transport as evidenced by order of magnitude increases in the eddy diffusivity. Measurements of the cross spectra of $\overline{v\theta}$, the vertical component of the turbulent heat flux, revealed a significant peak at frequencies associated with vortex shedding from the obstacle, suggesting that large-scale unsteadiness associated with vortex shedding was contributing to the increase in heat transport within the boundary layer. This unsteady behavior was clearly distinct from the low-frequency phenomena observed by Rood and Keller (1984), because it was identified outside as well as inside the boundary layer.

The presence of shed vortices in the downstream boundary layer can be thought of as a type of *locally* periodic unsteadiness, because only a portion of the flow field is affected by the unsteadiness. The term local distinguishes such situations from *globally* periodic flows, in which the entire flow field is modulated, i.e., pulsatile and oscillatory flows.

Despite the prevalence of junction flows, little is known about the effect of local unsteadiness on heat transfer. Even in the few studies for which detailed turbulence data are available, the unsteadiness is most often treated as a component of the turbulence. Unfortunately, applying the traditional experimental methods for stationary turbulent flows can mask the physical mechanisms associated with the periodic motion. The objective of the current work is to separate the heat transport attributable to the large-scale periodic unsteadiness from that attributable to the turbulence by analyzing detailed temperature and velocity data with a combination of conditional sampling and triple decomposition techniques.

Data analysis techniques

Experimental data

The tests were performed in an open-loop, blower-driven, wind-tunnel facility at the University of California, Berkeley. The test section is 76.2 cm in width and 22.9 cm high. The approaching thermal and momentum boundary layers developed initially over a heated entrance section, 121.9-cm long, with a boundary layer trip at its entrance. The cylinder, with a chord length of 8.9 cm and a leading-edge diameter of 3.8 cm, was situated downstream of the entrance section on an unheated floor hatch, with its leading edge 134.9 cm from the boundary-layer trip. The downstream junction boundary layer developed over another heated section 156.9-cm long; data were obtained over this section, across a plane located 189 cm from the boundary-layer trip, corresponding to 54.1 cm (14 diameters) downstream of the leading edge of the cylinder. The heated floor sections consisted of etched foil heater elements, embedded within a flexible silicone rubber jacket and covered with a smooth 0.2-mm thick stainless steel foil. The convective heat flux from the surface of the heaters (accounting for radiation losses) was 350 W/m^2. The flow had a reference velocity of 10 m/s, measured in the free stream near the boundary-layer trip, resulting in $Re_D = 24{,}700$.

Simultaneous velocity and temperature measurements were obtained using a triple-wire heat-flux probes, which consisted of two constant-temperature hot wires, operated with an overheat ratio of 0.8, arranged in an X-wire configuration. In between and

Notation

D	base diameter of streamlined cylinder, m
f	frequency, Hz
k	threshold level for conditional sampling
N	number of periodic cycles
STV	short time variance, Equation 6
t	time, s
t_i	reference time for the ith periodic event, s
U, V, W	instantaneous velocity components, m/s
u, v, w	fluctuating velocity components, m/s
$\overline{uv}$, $\overline{uw}$	overall Reynolds stresses, m^2/s^2
$\overline{v\theta}$, $\overline{w\theta}$	overall Reynolds heat fluxes, °C m/s

Greek

δ	boundary layer thickness, m
γ	intermittency of temperature signal
Θ	instantaneous temperature,°C
θ	fluctuating temperature,°C
τ	time relative to reference point in periodic cycle, s

Superscripts and overlines

$'$	fluctuation about ensemble-averaged mean
$\tilde{}$	ensemble average, Equation 2
$\bar{}$	time average

in a plane parallel to the X-wires, was a constant-current cold wire, used to measure temperature. All three sensors of the heat-flux probes were 2.5-μm diameter tungsten, with an active length of $l/d = 280$ ($l/y^* = 201$ and $l/\delta = 0.015$) * and wire-to-wire spacing of $s = 0.35$ mm ($s/y^* = 100$ and $s/\delta = 0.0075$). The wire ends were plated with 24-μm diameter copper plating, which extended the overall wire length to 3.3 mm for the X-wire sensors, and to 2.2 mm for the cold wire. One probe was made up of sensors oriented in a vertical position, to measure U, V, and Θ, while the other consisted of horizontally mounted sensors to measure U, W, and Θ. Data were taken on only one side of the wake, with both probes, assuming that the flow would be nearly symmetrical around the spanwise centerline of the tunnel. The heat-flux-probe X-wires were operated by DISA 56C17/56C01 constant temperature anemometer (CTA) systems and a DISA 56C20 temperature bridge provided a constant-current system for the cold wires. The signal outputs were sampled and digitized at a frequency of $f_s = 6000$ Hz ($f_s y^*/u_\tau = 0.55$, $f_s\delta/U_\infty = 21.1$) for a sampling time of $T_s = 5.5$ seconds ($T_s u_\tau/y^* = 60{,}000$, $T_s U_\infty/\delta = 1560$).

An analytical technique was employed to compensate for the reduced frequency response of the constant-current cold wire, accounting for both end-conduction and wire-thermal-inertia effects (Wroblewski and Eibeck 1991a). These corrections are important for conditional sampling studies, in order to clearly identify the sharp interface between hot, turbulent fluid and cold free-stream fluid. Further details of the experimental setup and instrumentation can be found in Wroblewski and Eibeck (1991a, 1992).

Previous analysis of the turbulence spectra indicated that the junction boundary layer at $x/D = 14$ could be characterized by three distinct spanwise regions (Wroblewski and Eibeck 1992): (1) the inner-wake region, $z/D < 0.8$, where unsteady effects are observed only in the spanwise component of the fluctuations; (2) the middle-wake region $0.8 < z/D < 1.8$, where strong unsteadiness is seen in all three components of the fluctuations and in the heat fluxes; and (3) the outer-wake region, $z/D > 1.8$, where the flow is approaching an undisturbed boundary layer, but still exhibits some modest effects from the unsteadiness.

The extent of these regions is shown in Figure 2, with contour lines for $\overline{v\theta}$, the vertical component of the Reynolds heat flux (including periodic motions and the turbulence). Note that the heat flux shows a peak value in the middle-wake at $z/D = 1.31$ and $y/D = 0.56$. The point labeled P, near the peak heat flux, was chosen for the development of the conditional sampling technique and is the main focus of the present study.

It should be noted that the measurement point nearest to the wall was located at 0.5 cm or $y^+ = 133$, near the outer edge of the log layer for the undisturbed flow. Therefore, the transport considered here is representative of the outer layer of the boundary layer.

Triple decomposition

In analyzing turbulent flows with large-scale periodic unsteadiness, the temperature and velocities are decomposed into three components, rather than the usual two components for classical Reynolds decomposition. Following Hussain and Reynolds (1970), the temperature for example, is expressed as follows:

$$\Theta(t) = \overline{\Theta} + \tilde{\theta}(\tau) + \theta'(t_i, \tau) \tag{1}$$

where $\overline{\Theta}$ represents the long time mean; $\tilde{\theta}(\tau)$ is the periodic mean (representing the periodic motions) as a function of τ (the time relative to some reference point in the periodic cycle); and $\theta'(t_i, \tau)$ represents the turbulent fluctuation about the periodic mean at a specific time, $t = t_i + \tau$, where t_i is the time corresponding to the reference point for the ith cycle. The total fluctuation about the long time mean is expressed as $\theta(t) = \tilde{\theta}(\tau) + \theta'(t_i, \tau)$.

Note that the overbar symbol ($\bar{}$) always denotes a time average, which results in a single value, while the tilde symbol ($\tilde{}$) always denotes an ensemble average, which results in a function of τ representing an "average" or typical cycle of the event. The periodic mean temperature profile is calculated from

$$\tilde{\theta}(\tau) = \frac{1}{N}\sum_{i=1}^{N} \theta(t_i, \tau) \tag{2}$$

where N is the total number of cycles.

The triple decomposition can be utilized to derive a modified form of the Reynolds-averaged equations. The streamwise momentum and the energy equations appropriate for a 3-D boundary-layer flow are as follows:

$$\frac{D\overline{U}}{Dt} = \frac{\partial}{\partial y}\left(\frac{\partial \overline{U}}{\partial y} - \overline{\tilde{u}\tilde{v}} - \overline{u'v'}\right) + \frac{\partial}{\partial z}\left(\frac{\partial \overline{U}}{\partial z} - \overline{\tilde{u}\tilde{w}} - \overline{u'w'}\right) \tag{3}$$

$$\frac{D\overline{\Theta}}{Dt} = \frac{\partial}{\partial y}\left(\frac{\partial \overline{\Theta}}{\partial y} - \overline{\tilde{v}\tilde{\theta}} - \overline{v'\theta'}\right) + \frac{\partial}{\partial z}\left(\frac{\partial \overline{\Theta}}{\partial z} - \overline{\tilde{w}\tilde{\theta}} - \overline{w'\theta'}\right) \tag{4}$$

where $\overline{\tilde{u}\tilde{v}}$, $\overline{\tilde{u}\tilde{w}}$, $\overline{\tilde{v}\tilde{\theta}}$, and $\overline{\tilde{w}\tilde{\theta}}$ represent the contributions to the Reynolds stresses and Reynolds heat fluxes attributable to the periodic motions, and $\overline{u'v'}$, $\overline{u'w'}$, $\overline{v'\theta'}$, and $\overline{w'\theta'}$ are the contributions attributable to the turbulent fluctuations. The periodic contributions to the transport are found by time-averaging the products of the periodic mean values. For example,

$$\overline{\tilde{v}\tilde{\theta}} = \int_0^T \tilde{v}(\tau)\tilde{\theta}(\tau)\, d\tau \tag{5}$$

where T is the period of the cycle. For the intermittently periodic behavior observed in the junction boundary layer, the typical cycle may include portions for which the periodic contributions are negligible. This can be accounted for in Equation 5 by multiplying by an intermittency factor that represents the fraction of the total sampling time for which periodic behavior is observed.

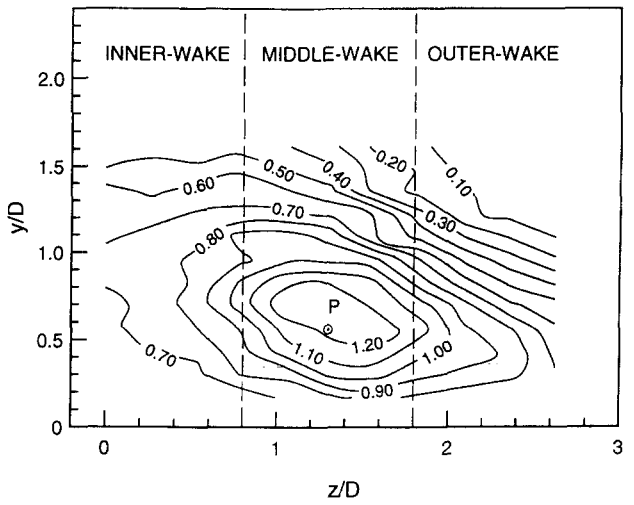

Figure 2 Isocontours of $\overline{v\theta}/(q_w/\rho c_p)$, vertical component of Reynolds heat flux, in z–y plane located at $x/D = 14$.

* All reference values of y^* and δ are for the undisturbed, flat-plate boundary layer.

Conditional sampling

In separating the large-scale motions from the background turbulence, a conditional sampling technique must be employed for two purposes: (1) to identify when an event is occurring; and (2) to identify a distinct reference point within each detected event so ensemble averaging can be performed. For pulsatile and oscillatory flows, both of these objectives can be achieved relatively easily through a timing signal from the mean flow. For intermittently periodic flows, such as the junction flow, a more general approach is required.

Figure 3 shows time series for u, v, and θ for point P within the middle-wake region (see Figure 2), where spectra indicated significant contribution from the large-scale unsteadiness with a frequency of approximately $f = 26$ Hz ($fy^*/u_\tau = 0.0024$, $f_s\delta/U_\infty = 0.09$). The temperature signal exhibits the most distinct signature for the periodic events (as indicated by the arrows)— a steep drop in temperature followed by a period of relatively constant temperature with very small fluctuations. By noting that this plateau level corresponds to the free-stream temperature, the sharp drop can be interpreted as the interface between the warm fluid in the thermal boundary layer and the cold free-stream fluid. This distinct feature of the temperature signal was utilized for identifying the occurrence of periodic events, as discussed below. Previous studies involving conditional sampling in boundary layers also used the temperature signal for event detection (Subramanian et al. 1982). Note, however, that in the present study, the main interest is not the structures of the flow field, but the characterization of the periodic events associated with the unsteady heat transport; the use of the temperature signal for identifying these events is justified, although the boundary conditions, and hence, the overall structure, of the momentum and thermal fields may be quite different.

The conditional sampling method that was employed involves the calculation of the short time variance (STV)

$$\mathrm{STV} = \frac{1}{T}\int_{t_1-T/2}^{t_1+T/2}\theta^2(t)\,\mathrm{d}t - \left[\frac{1}{T}\int_{t_1-T/2}^{t_1+T/2}\theta(t)\,\mathrm{d}t\right]^2 \qquad (6)$$

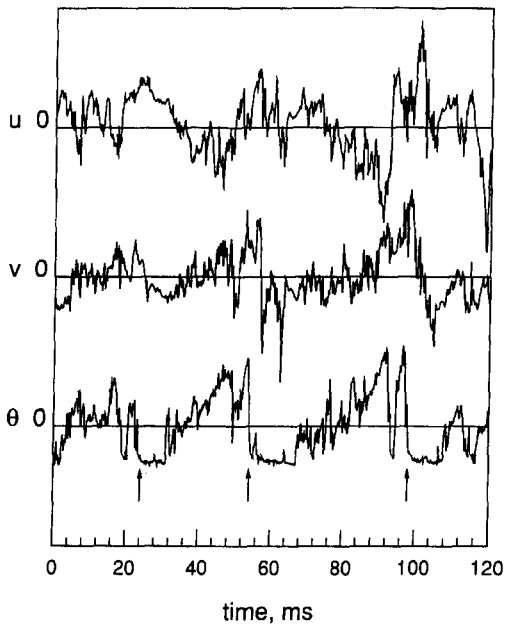

Figure 3 Typical time series for u, v, and θ at $z/D = 1.31$ and $y/D = 0.56$; arrows identify passing of temperature interface that characterizes periodic events.

which represents the variance of a signal over some time period T centered at time t_1. The short time variance attains significant levels during events with periods approximately equal to the averaging time, and forms the the basis of the variable integral time average (VITA) technique that has been successfully used to identify near-wall events in turbulent boundary layers (Blackwelder and Kaplan 1976). In the junction boundary layer, the events to be detected display periodic behavior, rather than the intermittent behavior associated with near-wall events, so it is unlikely that the standard VITA technique would be appropriate. Instead, the short time variance was employed in a method that exploits the characteristic temperature drop associated with the unsteady motions (Figure 3). This method involved three steps.

First, the temperature signal was passed through a band-pass filter to isolate motions within a bandwith surrounding the frequency of the periodic motions. The idea is to clearly identify zero-crossings associated with the periodic motions, while eliminating those attributable to the turbulent fluctuations. This was accomplished by performing a fast Fourier transform (FFT) on the entire signal span, spectrally filtering the transformed signal using the complex response function for the filter, and applying an inverse FFT to recover the filtered time series. The band-pass filter had cutoff frequencies of 6 and 100 Hz.

Second, all zero crossings with a negative slope were identified from the filtered signal. The negative sloped crossings were selected (as opposed to the positive slope crossings), because they mark a distinguishing feature of the event, as discussed above. For each zero crossing, the STV was calculated with a period of 38.3 ms centered on the zero crossing. If the STV exceeded some threshold level times the long-time variance of the filtered signal, $\mathrm{STV} > k(\theta)^2$, then a periodic event was considered to have occurred, and the zero crossing was marked as the reference point. Note that the STV was used in a manner different than the standard VITA technique, in which it is used to identify appropriate events and to locate a suitable reference point. Here, its purpose was to distinguish zero crossings associated with large-scale periodic events (with a frequency of approximately 26 Hz) from those that might be associated with more rapid fluctuations that are not removed by filtering.

Third, the unfiltered temperature and velocity signals were ensemble averaged over all detected events (typically around 100), to obtain the periodic mean values, $\tilde{u}$, $\tilde{v}$, $\tilde{w}$, and $\tilde{\theta}$. Values of the periodic contributions to the Reynolds stresses and heat fluxes were calculated from the periodic mean results (Equation 5, for example). Turbulence quantities were obtained by subtracting the periodic mean from the signal and ensemble averaging the result. For example, the ensemble averaged variance of turbulent temperature fluctuations is given by the following;

$$\widetilde{(\theta')^2}(\tau) = \frac{1}{N}\sum_{i=1}^{N}\left[\theta'(t_i,\tau)\right]^2 \qquad (7)$$

Results

Threshold-level sensitivity

The threshold level k was selected based on a sensitivity analysis using the data at the location of the peak heat fluxes. Figure 4 shows the variations in the $\overline{\tilde{u}\tilde{v}}$, $\overline{\tilde{u}\tilde{u}}$, $\overline{\tilde{v}\tilde{v}}$ $\overline{\tilde{\theta}\tilde{\theta}}$, and $\overline{\tilde{v}\tilde{\theta}}$ with the threshold level. Note that values for all quantities, which represent the contribution from the periodic motions to the particular overall Reynolds stress or heat flux, are approximately constant within the range $0.8 < k < 1.0$, with the maximum values occurring at $k = 0.9$. With threshold levels below this range, more events are detected, but these are not necessarily associated with

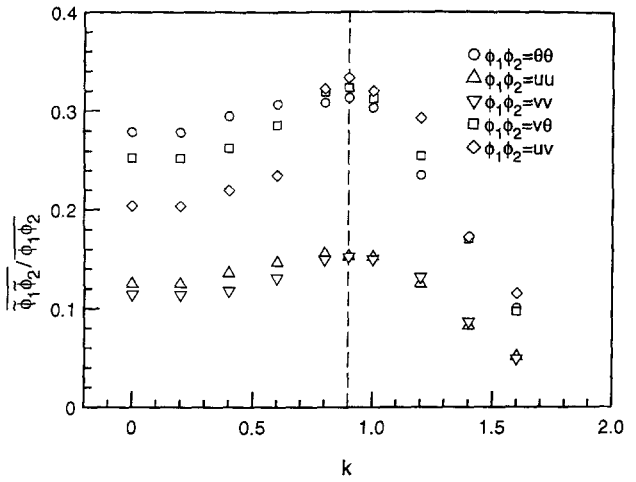

Figure 4 Effect of threshold level k on the calculation of periodic contributions to the Reynolds stresses and Reynolds heat fluxes.

the periodic motions, and the resulting ensemble-averaged values are smaller. For higher threshold levels, fewer events are detected, so that the contribution to the overall stresses or heat fluxes are also smaller. The existence of this plateau level suggests that a threshold level within this range would be appropriate. Because capturing the transport attributable to the periodic motions is the main objective of this work, and the calculated transport is maximum for $k = 0.9$, it was decided that a threshold level of 0.9 would be used.

Ensemble averages

Ensemble-averaged mean values are presented in Figure 5 for $z/D = 1.31$ and $y/D = 0.56$. The temperature signal θ is characterized by a gradual increase to a peak value, followed by an abrupt drop to a near constant level near the ambient temperature, before gradually increasing again. This is accompanied by an analogous, but opposite, trend in $\tilde{u}$. This distinct feature, as discussed above, is likely associated with the interface between the low momentum, warm near-wall fluid and the high momentum, colder free-stream fluid.

The warm side of the front is associated with an upwash ($\tilde{v} > 0$) and outwash ($\tilde{w} > 0$) of fluid, while the cooler side

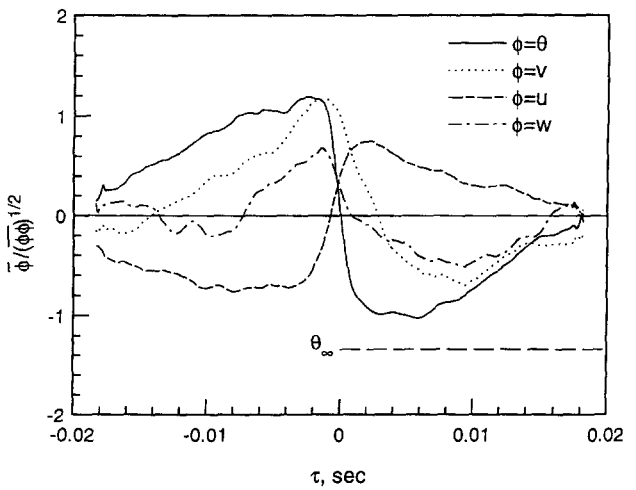

Figure 5 Ensemble-averaged mean profiles for temperature and velocities at $z/D = 1.31$ and $y/D = 0.56$.

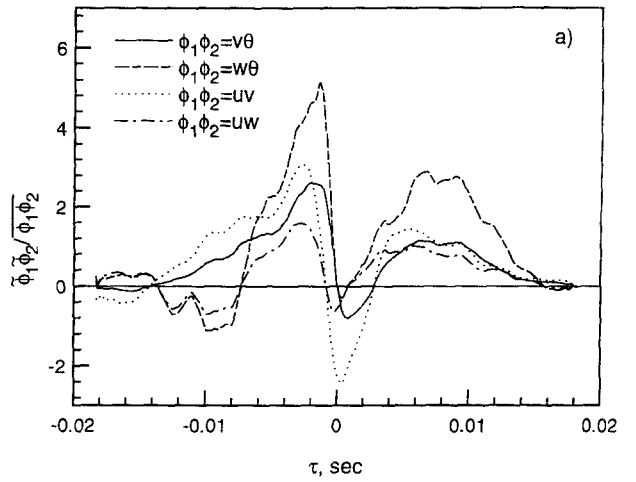

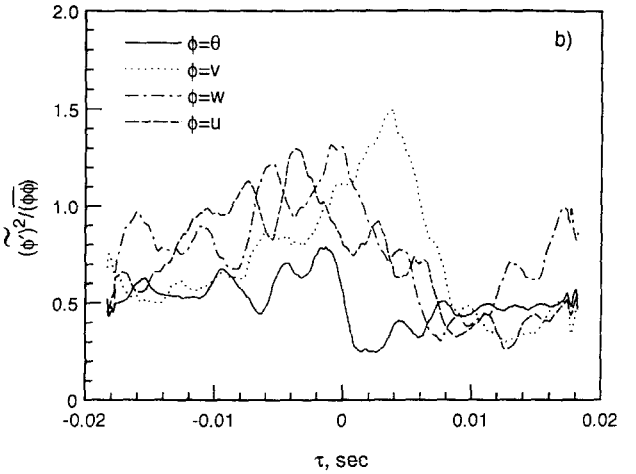

Figure 6 Ensemble-averaged profiles at $z/D = 1.31$ and $y/D = 0.56$: a) Reynolds stresses and Reynolds heat flux; b) turbulent fluctuation variances for temperature and velocities.

exhibits predominantly downwash and inwash of fluid. This type of behavior suggests that a vortex passes by the probe and convects cooler, high momentum fluid toward the wall in its downwash zone and convects high temperature, low momentum fluid away from the wall in its upwash zone. However, note the $\tilde{v}$ lags $\tilde{\theta}$, and the interface actually passes the probe during an upwash, suggesting cooler fluid moving away from the wall for a short period (approximately 2.5 ms). It may be argued that the behavior of the velocity during a typical cycle; i.e., the downwash followed by an upwash, is an artifact of the choice of sampling technique. However, the presence of the downwash and reverse transport during the interface passing suggests that the conditional sampling and ensemble averaging are revealing a physical phenomenon not usually associated with turbulent heat transport in undisturbed boundary layers. This aspect of the unsteady motion is discussed in more detail below.

The ensemble-averaged Reynolds shear stresses and heat fluxes (which represent the transport of momentum and heat by the periodic motions) are plotted in Figure 6a as a function of τ. These results indicate a strong tendency for the periodic motions to transport heat and momentum, confirming the previously reported assertion that the unsteadiness played a key role in the transport (Wroblewski and Eibeck 1992). The vertical component of the heat flux $\tilde{v}\tilde{\theta}$ is predominantly positive, and the vertical component of the Reynolds shear stress $\tilde{u}\tilde{v}$ is predominantly

negative, consistent with undisturbed turbulent boundary-layer trends. However, near $\tau = 0$, "reverse transport" is observed for a short period. This arises because of the lagging $\tilde{v}$, as mentioned above, leading to a period when low-temperature, high-momentum fluid is actually transported away from the wall.

The ensemble-averaged variances of the turbulent fluctuations, which represent the level of fluctuations about the ensemble-averaged mean values shown in Figure 5, appear in Figure 6b. The upwash portion of the cycle, before the front passes at $\tau = 0$, is characterized by elevated levels of fluctuations in u', w', and θ'. This is consistent with the idea of near-wall fluid (characterized by higher level of wall-generated turbulence) being convected away from the wall region. The drop in these levels after the front has passed represents lower turbulence levels characteristic of outer layer fluid being transported downward. In particular, the very low level of temperature fluctuations right after the interface passes is associated with the fluid outside the thermal layer.

To check whether the periodic events identified by the conditional sampling technique are associated with the unsteadiness from the vortex shedding, and not with motions characteristic of normal boundary layer turbulence, the technique was applied to data obtained with no obstacle present, at the same streamwise plane. Ensemble-averaged mean values and the transport associated with the detected events are shown in Figure 7a for $y/\delta =$ 0.56, the same y location as the data described above. Although the ensemble mean values exhibit some general similarities to the junction flow results, this is to be expected, given that the event detection searches for zero crossings. However, there are some key differences: (1) the minimum temperature is well above the ambient, indicating that motions are not associated with the movement of the instantaneous interface; (2) the period of the events is shorter; (3) $\overline{\tilde{u}\tilde{v}}$ and $\overline{\tilde{v}\tilde{\theta}}$ do not exhibit "reverse" transport near $\tau = 0$; and (4) the contribution to the overall transport is relatively small (the contribution to $\overline{v\theta}$ is only 5% compared to 30% for the junction boundary layer). Most likely, at this location, the conditional sampling is separating the large-scale, passive motions of the turbulence in the boundary layer from the transport-producing integral scales.

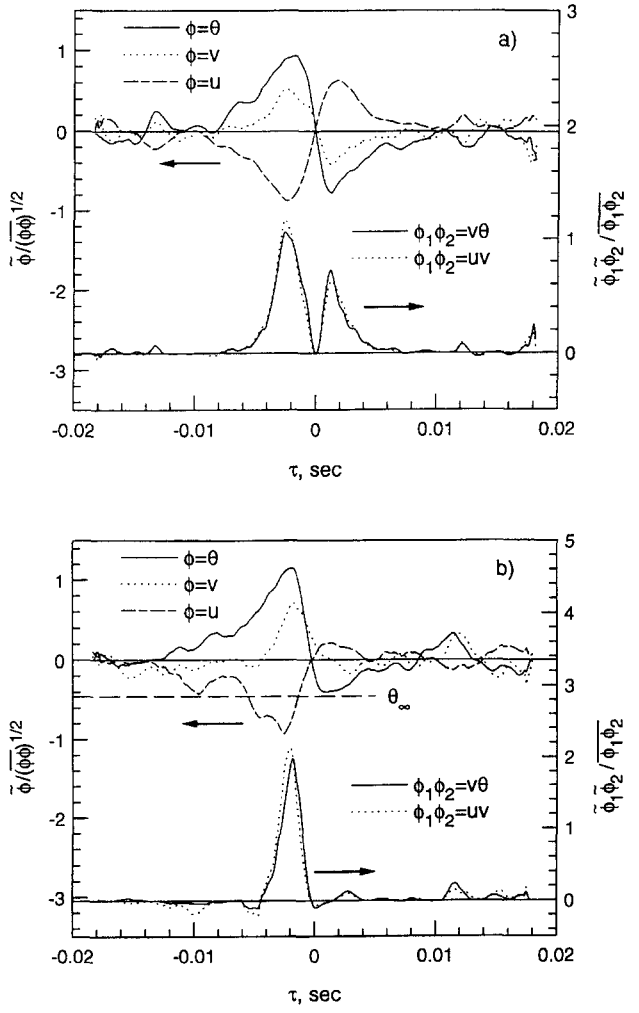

Figure 7 Ensemble-averaged mean and Reynolds transport profiles for 2-D (undisturbed) boundary layer at $z/D = 1.31$: a) $y/D = 0.56$; b) $y/D = 0.97$.

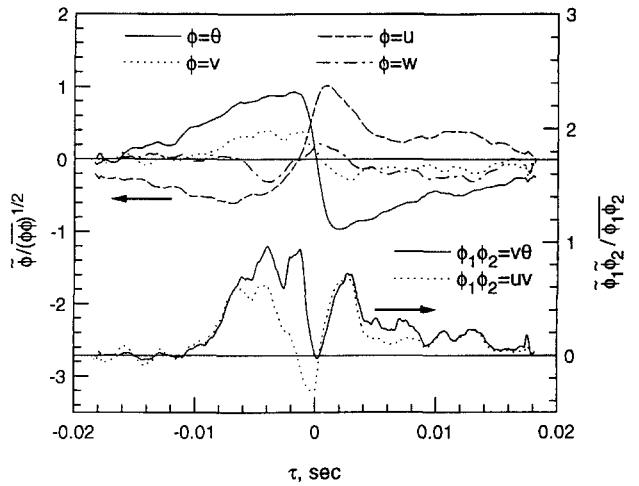

Figure 8 Ensemble-averaged mean and Reynolds transport profiles at $z/D = 1.31$ and $y/D = 0.17$.

At $y/\delta = 1.0$ (Figure 7b), a location in the highly intermittent region of the undisturbed boundary layer, the detected events are most likely "bulges" of the warm, turbulent fluid at the edge of the boundary layer as they pass the probe. The sharp increase in temperature before the peak temperature is reached marks the leading edge of a bulge. Note that the temperature is not equal to the ambient temperature preceding this leading edge. This is because the bulges are of varying duration; the ensemble-averaging, referenced to the negatively sloped zero crossing, averages the higher temperatures associated with longer bulges with lower, ambient temperatures associated with shorter bulges. In contrast, events observed in the junction flow have nearly the same duration, characteristic of their periodic nature. Transport attributable to these detected events is observed only during the leading edges of the bulge, with no reverse transport near the interface crossing, also distinctly different from the junction flow.

It should be noted that because no periodic structures are present in the *undisturbed* boundary layer, the application of the event-detection and ensemble averaging is not strictly appropriate, because it was developed primarily for identifying periodic motions. It is utilized for the undisturbed flow solely as a means to demonstrate that the events detected in the junction flow are not merely artifacts of the boundary-layer turbulence, but are unique to the periodic motions, particularly with regard to the behavior during the passing of the instantaneous temperature interface.

Ensemble averages and resulting transport obtained at a point nearer to the wall in the middle-wake region, appear in Figure 8. The pattern of the periodic motion differs from the peak-heat flux point in two key aspects. First, the minimum temperature is far from the free-stream levels (the free-stream temperature corre-

sponds to $\theta_\infty = -2.4°C$ in the figure), indicating that the instantaneous interface does not penetrate that deeply into the wall layer. Second, the ensemble-averaged transport is smaller and does not exhibit reverse heat transport near $\tau = 0$. These characteristics are somewhat reminiscent of the behavior observed in the two-dimensional (2-D) boundary layer (Figure 7), suggesting that the near-wall region may be influenced by wall-bounded turbulence behavior as well as by the large-scale periodic motions seen in the outer layer.

Results for other locations within the flow field at $x/D = 14$ (not shown) reveal behavior similar to that observed in the middle-wake region. In particular, the temperature interface passing is accompanied by an upwash at all spanwise locations, for $0.3 < y/D < 1.3$.

Reynolds heat fluxes and intermittency

The total contributions to Reynolds heat fluxes from the periodic motions (defined in Equation 5) are shown in Figure 9 for the entire y–z plane. These exhibit a maximum near the point of peak total heat flux, in the middle-wake region, accounting for 30% of $\overline{v\theta}$, and 54% of $\overline{w\theta}$ at that location. This confirms the suggestion that the periodic unsteadiness is largely responsible for these peak values. Near the wall, in the outer-wake zone, the periodic motions lead to negative (inward) spanwise heat transport. From a gradient transport point of view, this is actually consistent with the mean temperature field, which exhibits positive $\partial\overline{\Theta}/\partial z$ in that region. Note that these results are for a threshold level of 0.9, and the values will likely decrease for other values of k, as shown previously in Figure 4.

Because the periodic events are characterized by large-scale movements of the instantaneous thermal interface, the temperature signal should have a distinctly intermittent nature. The intermittency γ is defined as the fraction of the time that the probe, at a given location within the flow field, is on the heated side of the interface. It is calculated from the temperature data, using the following;

$$\gamma = \frac{1}{N_s}\sum_{n=1}^{N_s} I_n$$

where N_s is the number of data samples, and $I_n = 1$ if $\Theta > \Theta_\infty$, and $I_n = 0$ otherwise.

Figure 10 displays the intermittency γ as a function of y/D for several values of z/D. The intermittent region is much larger, and the temperature interface penetrates much deeper into the boundary layer when compared to the undisturbed flow. The deepest penetration occurs in the middle-wake region ($z/D = 1.31$ in Figure 10), where the unsteady motions are most significant.

In the undisturbed boundary layer, the profile of γ *versus* y can be expressed in terms of a complementary error function (Klebanoff 1954). This indicates that the instantaneous position of the interface has a Gaussian, or random nature, with the mean location of the interface located at the point where $\gamma = 0.5$. ($y/D = 0.847$ for this undisturbed flow). In contrast, intermittency values from the junction boundary layer are not well fit to a complementary error function in the regions where the unsteady effect is predominant (e.g., middle wake). This might be expected, because the interface motion is controlled by a relatively coherent periodic motion, rather than by the somewhat random movement of the turbulent bulges in an undisturbed boundary layer.

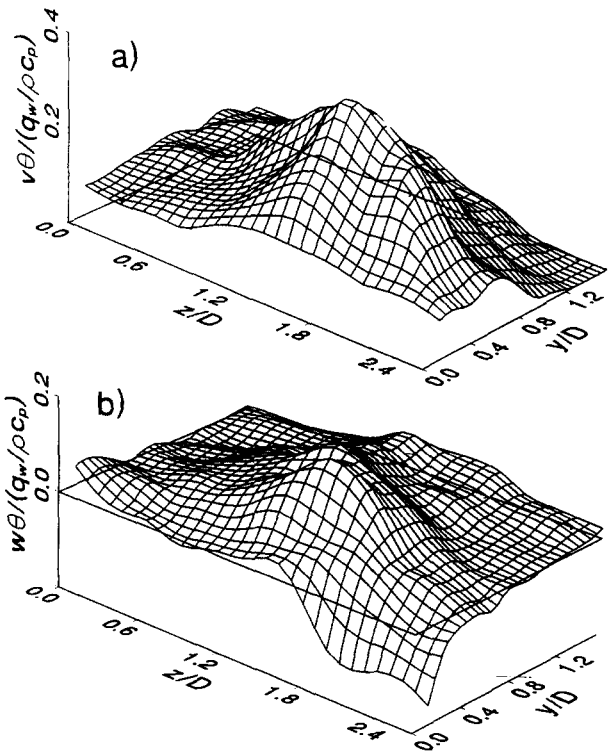

Figure 9 Reynolds heat fluxes attributable to periodic motions for z–y plane at $x/D = 14$: a) $\overline{\tilde{w}\tilde{\theta}}/(q_w/\rho c_p)$, spanwise component; b) $\overline{\tilde{v}\tilde{\theta}}/(q_w/\rho c_p)$, vertical component.

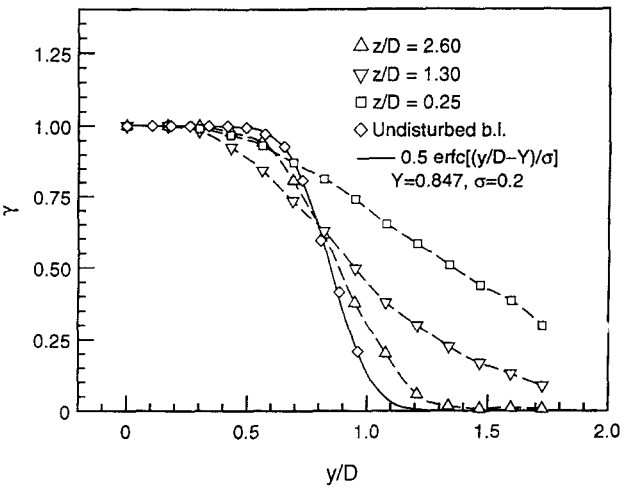

Figure 10 Intermittency of temperature signal *versus* y/D.

Discussion

The frequency of the periodic behavior suggests that vortex shedding plays a role in the large-scale transport. The ensemble-averaged data presented above suggest two possible mechanisms for this observed transport phenomena: (1) a portion of the skewed shed vortex filament itself, or (2) periodic spanwise oscillations of the large counter-rotating streamwise vortex.

Shed vortex effect

Consider a shed vortex as a vortex filament initially oriented in the vertical direction. As the vortex is convected downstream, it is "bent" by the action of the mean shear, primarily by the boundary-layer shear. A fragment of the skewed filament can

convect near-wall fluid away from the wall in its upwash region and cooler outer-layer fluid toward the wall in its downwash region. If the vortex is strong enough, it can actually begin to roll up the thermal interface (Figure 11). The behavior observed in the ensemble-averaged data is associated with the thermal interface wrapped around the skewed vortex filament as it washes over the probe. The larger intermittent region arises because of the relatively large size of the shed vortex compared to the thermal-layer thickness, resulting in large-scale vertical movement of the interface.

This model also may explain the fact that the interface passes during an upwash phase, leading to a short period of "negative" heat fluxes. The particular plane of data discussed here may be far enough downstream that the vortex wraps the cold fluid around its core and into the upwash region (Figure 11), accounting for the transport of cool, high-momentum fluid away from the wall near $\tau = 0$.

It should be noted that this is an extremely complex flow, and such a simplistic model is only a "cartoon" that describes the more salient features of the observed data. The actual shape and orientation of a shed vortex filament is expected to be quite complex because of several factors: (1) a complicated mean secondary flow field characterized by a weak horseshoe vortex near the wall and a larger vortex observed away from the wall; (2) the self-induced flow field that arises as the filament is bent; (3) the induced flow field from its image vortex that arises because of the proximity to a solid wall; and (4) the fluctuating strain field from the turbulence.

Counter-rotating vortex effect

Another possible explanation for the observed results involves the large swirling vortices observed behind the obstacle (Wroblewski and Eibeck 1992). It is possible that these vortices are oscillating in the spanwise direction in the unsteady wake of the obstacle as a result of the periodic vortex shedding. The idea of the oscillating vortex is supported in part by the mean streamwise vorticity $(\partial\overline{W}/\partial y - \partial\overline{V}/\partial z)$ results, shown in Figure 12. The vorticity was calculated by fitting the secondary velocities at each y location and each z location with fourth-order polynomials and differentiating these to obtain the necessary gradients. Figure 12 indicates that the positive vorticity contours are elliptical rather than circular in shape. Elliptical-shaped vorticity contours have been observed in a boundary layer with an embedded streamwise vortex that is oscillating lateral to the flow (Westphal and Mehta 1987).

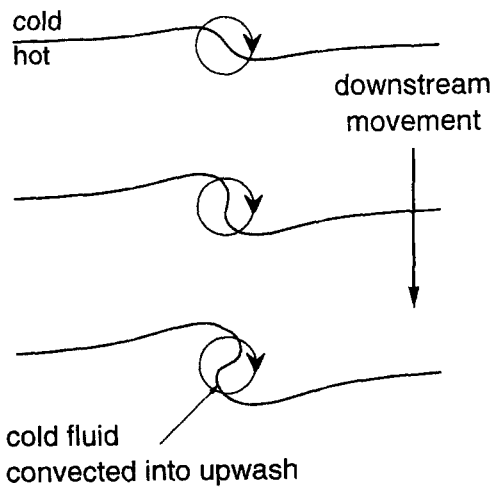

Figure 11 Schematic of roll-up of temperature interface by vortex filament.

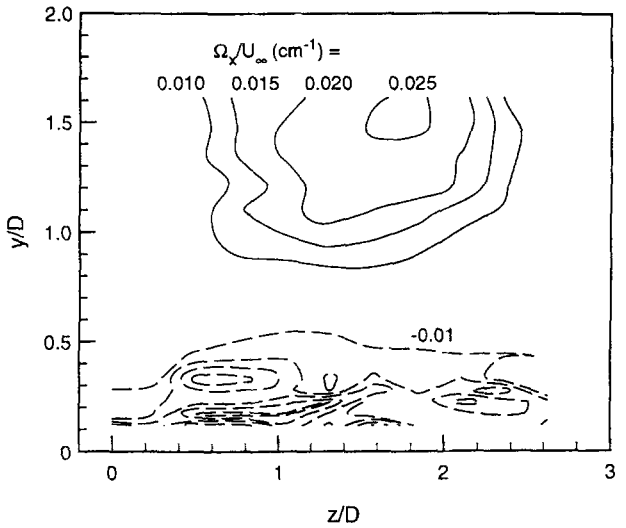

Figure 12 Isocontours of mean streamwise vorticity in $z-y$ plane located at $x/D = 14$; negative contours (dashed lines) are shown every $\Omega_x/U_\infty = 0.01$ starting with -0.01.

The large-scale streamwise vortices could also wrap up the temperature interface as the flow progresses downstream (Figure 11). In this case, the interface would move laterally during the vortex oscillation, as opposed to the proposed vertical motion suggested by the shed vortex model discussed above. The most significant effect of such oscillations on the transport and the deepest penetration of the interface would be expected in the region below the vortex center, at around $z/D = 1.5$, because the thermal interface would most likely pass through the center as it is wrapped up by the vortex. This is consistent with the observed results.

A third potential mechanism, which may be unrelated to vortex shedding, involves the viscous eruptive effect, in which an adverse pressure gradient caused by a near-wall vortex causes the surface layer to be lifted away from the wall. Smith et al. (1991) have shown that in a laminar horseshoe vortex system around a circular cylinder, the legs of the horseshoe vortex generate these surface eruptions, which can eventually evolve into a train of hairpin vortices convecting downstream along the upwash side of the vortex leg. If these eruptions are present in the turbulent junction boundary layer, they may be a contributing factor to increased wall heat transfer. However it seems unlikely whether these eruptions and the subsequent hairpin vortices could be the cause of the unsteady motions observed here, because the unsteady motions seem to be strongest in the outer region away from the wall. In particular, the unsteadiness is observed well outside the boundary layer, where the near-wall structures would not exert a significant influence.

The type of behavior discussed here is expected to occur, to some degree, in the junction boundary layer behind any bluff object near a wall. If the periodic behavior is due to the shed vortex itself, then the extent to which the thermal boundary layer is affected will depend upon the relative size of the obstacle (which determines the size of the vortex) compared to the thermal boundary-layer thickness. In the present study $D/\delta = 1.45$, where δ is the undisturbed thermal boundary layer thickness at the leading edge of the obstacle. If the large streamwise vortex is responsible, then the scaling may be more complicated, because the tunnel height, which determines the size of the vortices, may also be important. In addition, heating of the obstacle will thicken the thermal layer considerably. In such cases, the periodic motions may not actually wrap up the inter-

face, but should still lead to increased transport in the downstream region.

It seems clear that vortex shedding from the obstacle can greatly affect the heat transport downstream of the junction. However, thus far there is insufficient evidence to answer two main questions: (1) which, if either, of the two mechanisms described above is most plausible, and (2) what is the effect of the unsteadiness on the wall heat transfer?

Acknowledgments

The experimental data discussed in this paper were obtained at the University of California, Berkeley, under grant DE-FG03-87ER 13780 from the Department of Energy's Office of Basic Energy Sciences and under the supervision of Professor Pamela Eibeck. Analysis of the data was supported in part by the Boston University College of Engineering and by the National Science Foundation under grant CTS-9211282.

References

Baker, C. J. 1980. The turbulent horseshoe vortex. *J. Wind Eng. Ind. Aerodynamics*, **6**, 9–23

Blackwelder, R.F. and Kaplan, R.E. 1976. On the wall structure of the turbulent boundary layer. *J. Fluid Mech.*, **76**, 89–112

Eibeck, P. A. 1991. An experimental study of the flow downstream of a circular and tapered cylinder. *J. Fluids Eng.*, **112**, 393–401

Eibeck, P. A. and Barland, D. E. 1993. Turbulent mixing behind two-dimensional and finite obstacle. *Turbulent Mixing*, ASME FED, **174**, 57–64

Fisher, E. M. and Eibeck, P. A. 1990. The influence of a horseshoe vortex on local convective heat transfer. *J. Heat Transfer*, **112**, 329–335

Goldstein, R. J. and Karni, J. 1984. The effect of a wall boundary layer on local mass transfer from a cylinder in crossflow. *J. Heat Transfer*, **106**, 260–267

Hussain, A. K. M. F. and Reynolds, W. C. 1970. The mechanics of an organized wave in turbulent shear flow. *J. Fluid Mech.*, **41**, 241–258

Klebanoff, P. S. 1954. Characteristics of turbulence in a boundary layer with zero pressure gradient. NACA Technical Note 3178

McMahon, H., Hubbartt, J. and Kubendran, L. 1983. Mean velocities and Reynolds stresses upstream of a simulated wing fuselage junction. NASA Contractor Report No. 3695, NASA-Langley Research Center, Hampton, VA

Mehta, R. D. 1984. Effect of wing nose shape on the flow in a wing/body junction. *Aeronautical J.*, **88**, 456–460

Merati, P., McMahon, H. M. and Yoo, K. M. 1988. Experimental modeling of a turbulent flow in the junction and wake of an appendage flat plate. *Proc. AIAA / ASME / SIAM / APS 1st Nat. Fluid Dynamics Congress*, Cincinnati, OH, 1255–1264

Pauley, W. 1993. The fluid mechanics and heat transfer downstream of struts spanning a low-aspect-ratio channel. Paper presented at the 1993 National Heat Transfer Conference, Atlanta, GA

Pierce, F. J. and Harsh, M. D. 1988. The mean flow structure around and within a turbulent junction or horseshoe vortex — Part II. The separated and junction vortex flow. *J. Fluids Eng.* **110**, 415–423

Rood, E. P. and Keller, J. E. 1984. Evidence of large-scale time-dependent flow in a wing–wall interaction wake. *Unsteady Turbulent Boundary Layers and Friction*, ASME FED, **12**, 39–44

Shabaka, I. M. M. A. and Bradshaw, P. 1981. Turbulent flow measurements in an idealized wing/body junction. *AIAA J.*, **19**, 131–132

Smith, C. R., Fitzgerald, J. P. and Seal, C. V. 1992. The development of flow structure in end-wall boundary layers: A metamorphosis of three-dimensional, unsteady behavior. *Proc. Conference on Turbulent Flows and VTSS Honoring Stephen J. Kline*, Stanford, CA, August 10–11

Smith, C. R., Walker, J. D. A., Haidari, A. H. and Sobrun, U. 1991. On the dynamics of near-wall turbulence. *Phil. Trans. R. Soc. Lond. A*, **336**, 131–175

Subramanian, C. S., Rajagopalan, S., Antonia, R. A., and Chambers, A. J. 1982. Comparisons of conditional sampling techniques in a turbulent boundary layer. *J. Fluid Mech.*, **123**, 363–378

Westphal, R. V. and Mehta, R. D. 1987. Interaction of an oscillating vortex with a turbulent boundary layer. *Proc. AIAA 19th Fluid Dynamics, Plasma Dynamics, and Lasers Conference* (AIAA Paper 87–1246)

Wroblewski, D. E. and Eibeck, P. A. 1991a, A frequency response compensation technique for cold wires and its application to a heat flux probe. *Exp. Thermal Fluid Sci.*, **4**, 452–463

Wroblewski, D. E. and Eibeck, P. A. 1991b. Measurements of turbulent heat transport in a boundary layer with an embedded streamwise vortex. *Int. J. Heat Mass Transfer*, **34**, 1617–1631

Wroblewski, D. E. and Eibeck, P. A. 1992. Turbulent heat transport in a boundary layer behind a junction of a streamlined cylinder and a wall. *J. Heat Transfer*, **114**, 840–849